[CANCER RESEARCH 64, 4251–4256, June 15, 2004]

Cellular Dynamics Visualized in Live Cells *in Vitro* and *in Vivo* by Differential Dual-Color Nuclear-Cytoplasmic Fluorescent-Protein Expression

Norio Yamamoto,[1,2,3] Ping Jiang,[1] Meng Yang,[1] Mingxu Xu,[1] Kensuke Yamauchi,[1,2,3] Hiroyuki Tsuchiya,[3] Katsuro Tomita,[3] Geoffrey M. Wahl,[4] Abdool R. Moossa,[2] and Robert M. Hoffman[1,2]

[1]AntiCancer, Inc., San Diego, California; [2]Department of Surgery, University of California, San Diego, California; [3]Department of Orthopedic Surgery, School of Medicine, Kanazawa University, Kanazawa, Ishikawa, Japan; and [4]The Salk Institute, La Jolla, California

ABSTRACT

We report here the genetic engineering of dual-color fluorescent cells with one color in the nucleus and the other in the cytoplasm that enables real-time nuclear-cytoplasmic dynamics to be visualized in living cells *in vivo* as well as *in vitro*. To obtain the dual-color cells, red fluorescent protein (RFP) was expressed in the cytoplasm of HT-1080 human fibrosarcoma cells, and green fluorescent protein (GFP) linked to histone H2B was expressed in the nucleus. Nuclear GFP expression enabled visualization of nuclear dynamics, whereas simultaneous cytoplasmic RFP expression enabled visualization of nuclear cytoplasmic ratios as well as simultaneous cell and nuclear shape changes. Thus, total cellular dynamics can be visualized in the living dual-color cells in real time. The parental HT-1080 and the derived dual-color clones had similar cell proliferation rates, suggesting that expression of GFP and/or RFP does not affect cell cycle progression. The cell cycle position of individual living cells was readily visualized by the nuclear-cytoplasmic ratio and nuclear morphology. Real-time induction of apoptosis was observed by nuclear size changes and progressive nuclear fragmentation. Mitotic cells were visualized by whole-body imaging after injection in the mouse ear. Common carotid artery injection of dual-color cells and a reversible skin flap enabled the external visualization of the dual-color cells in microvessels in the mouse brain where extreme elongation of the cell body as well as the nucleus occurred. Dual-color cells in various positions of the cell cycle were visualized in excised mouse lungs after tail-vein injection of the dual-color cells. In the lung, the dual-color cells were observed frequently juxtaposing their nuclei, suggesting a potential novel form of cell-cell communication. The dual-color cells thus are a useful tool for visualizing living-cell dynamics *in vivo* as well as *in vitro*. Drugs that could specifically perturb these processes can now be readily screened in real time *in vivo*.

INTRODUCTION

Visualization of microscopic cancer is essential for the understanding and control of cancer dormancy, growth, and colonization of distant sites (1). Several approaches involving tumor-cell labeling have been developed for visualizing tumor cells *in vivo*. The *Escherichia coli* β-galactosidase (*lacZ*) gene has been used to detect micrometastases (2). However, *lacZ* detection requires extensive histological preparation and sacrifice of the tissue or animal. Therefore, other techniques are required for real-time imaging and study of tumor cells in viable fresh tissue or living animals.

Use of skin-fold chambers, exteriorization of organs, and s.c. windows inserted with semi-transparent material (3–5) has yielded insights into microscopic tumor behavior. However, these techniques are only suitable for ectopic models (3) or for investigations with short periods of observation (4, 5). The difficulties of maintaining windows or other devices that are made with heavy, stiff, or other types of foreign materials limit the length of time that these tools can be used *in vivo* (3, 4). Cutaneous windows made with polyvinyl chloride film become opaque or detached after time, which precludes their use in long-term studies (4). However, in mice with green fluorescent protein (GFP)-expressing tumors, gene expression, angiogenesis, and physiological properties were studied by use of the dorsal skin-chamber combined with multiphoton confocal microscopy (3). A disadvantage to this technique is that the chamber limits investigation to the ectopic primary tumor.

Mice bearing GFP-expressing microscopic tumors on exteriorized organs can be examined with intravital microscopy. However, with this approach, the mice tend not to survive long enough to enable spatial-temporal studies of tumor dormancy, progression, and metastasis (5).

Another approach for visualizing tumor cells *in vivo* involves insertion of the luciferase gene into tumor cells causing them to emit light (6). However, once transferred to mammalian cells, luciferase enzymes require exogenous delivery of their luciferin substrate, which is an impractical procedure in an intact animal. Because of the low image resolution and signal achieved with this approach, it takes a substantial amount of time to collect sufficient photons to form an image from an anesthetized animal (6). The low image resolution of luciferase imaging does not enable precise localization of the signal. Also, whether luciferase can function stably *in vivo* has been called into question (7).

To externally image and follow the natural course or impediment of tumor progression and metastasis, high specificity and sensitivity, a strong signal, and high resolution are necessary. The *GFP* gene, cloned from the bioluminescent jellyfish *Aequorea victoria* (8), was chosen to satisfy these conditions because it has great potential for use as a cellular marker (9, 10). GFP cDNA encodes a 283-amino acid monomeric polypeptide with M_r 27,000 (11, 12) that requires no other *A. victoria* proteins, substrates, or cofactors to fluoresce (13). Gain-of-function bright mutants expressing the *GFP* gene have been generated by various techniques (14–16) and have been humanized for high expression and signal (17). Red fluorescent proteins (RFP) from the *Discosoma* coral have similar features as well as the advantage of longer-wavelength emission (18–20).

We have developed a whole-body imaging of metastases in mice by use of tumor cells expressing GFP and RFP. Fluorescence imaging presents many new possibilities including real-time studies of tumor progression, metastasis, and drug-response evaluations. With these fluorescent tools, single cells from tumors and metastases can be imaged. GFP technology has also been used for real-time imaging and quantification of angiogenesis (21).

GFP tagging also enabled visualization of specific chromosomal regions (22–24). A fusion protein of GFP and yeast histone H2B localized in yeast nuclei (25). A fusion protein of GFP and human histone H2B (H2B-GFP) was incorporated into nucleosome core particles of HeLa cells without perturbing cell cycle progression (26).

Received 2/25/04; accepted 3/22/04.

Grant support: National Cancer Institute Grants 1 R43 CA099258-01, 1 R43 CA103563-01, and 1 R43 CA101600-01.

The costs of publication of this article were defrayed in part by the payment of page charges. This article must therefore be hereby marked *advertisement* in accordance with 18 U.S.C. Section 1734 solely to indicate this fact.

Requests for reprints: Robert M. Hoffman, AntiCancer, Inc., San Diego, CA 92111. Phone: (858) 654-2555; Fax: (858) 268-4175; E-mail: all@anticancer.com.

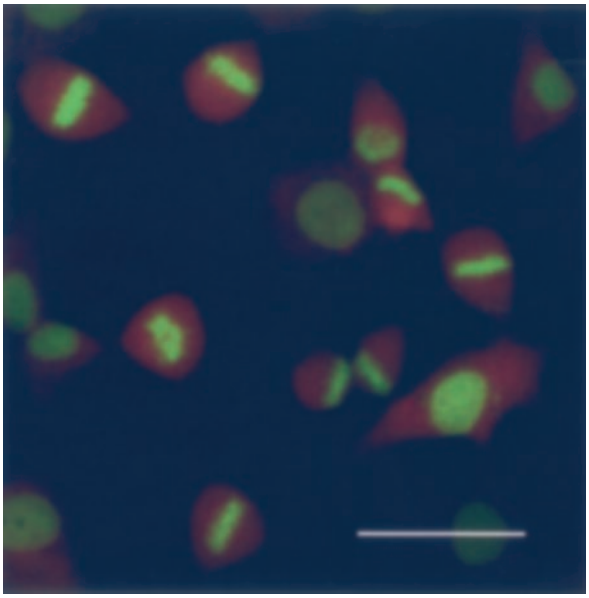

Fig. 1. Stable high GFP- and RFP-expressing human fibrosarcoma cells *in vitro*. Human fibrosarcoma cells (HT-1080) were initially transduced with RFP and the neomycin resistance gene. The cells were subsequently transduced with histone H2B-GFP and the hygromycin resistance gene on a retrovirus vector. Double transformants were selected with G418 and hygromycin, and stable clones were established. See "Materials and Methods" for details. *Bar* = 50 μm.

H2B-GFP allowed high-resolution imaging of both mitotic chromosomes and interphase chromatin in live cells (27).

The visualization of nuclear cytoplasmic dynamics in living cells could enable the real-time study of the normal and malignant cell cycle and apoptotic behavior *in vivo* as well as *in vitro*. Chambers *et al*. (28) and Naumov *et al*. (5) used GFP-tagged tumor cells and intravital imaging to visualize individual cells. These studies visualized the shape of metastatic tumor cells *in vivo* but could not visualize nuclear-cytoplasmic dynamics, or nuclear shape changes, because the nucleus and cytoplasm could not be distinguished.

With only H2B-GFP labeling of cells, an overlay with differential interference contrast images along with the GFP fluorescence images was necessary to visualize nuclear-cytoplasmic morphology. The present study uses H2B-GFP and RFP to differentially label the nucleus and cytoplasm of human HT-1080 human fibrosarcoma cells. This strategy allows the visualization of the cell cycle, apoptosis, and nuclear deformability in live cells in real time. This dual-color tagging strategy also enables real-time observation of nuclear-cytoplasmic dynamics *in vivo* as well as *in vitro*.

MATERIALS AND METHODS

Production of RFP Retroviral Vector. For RFP retrovirus production (29), the *Hin*d III/*Not*I fragment from pDsRed2 (Clontech Laboratories, Inc., Palo Alto, CA), containing the full-length RFP cDNA, was inserted into the *Hin*d III/*Not*I site of pLNCX2 (Clontech Laboratories, Inc.) that has the neomycin resistance gene to establish the pLNCX2-DsRed2 plasmid. PT67, an NIH3T3-derived packaging cell line (Clontech Laboratories, Inc.) expressing the 10 Al viral envelope, was cultured in DMEM (Irvine Scientific, Santa Ana, CA) supplemented with 10% heat-inactivated fetal bovine serum (FBS; Gemini Bio-products, Calabasas, CA). For vector production, PT67 cells, at 70% confluence, were incubated with a precipitated mixture of LipofectAMINE reagent (Life Technologies, Inc. Grand Island, NY), and saturating amounts of pLNCX2-DsRed2 plasmid for 18 h. Fresh medium was replenished at this time. The cells were examined by fluorescence microscopy 48 h post-transduction. For selection of a clone producing high amounts of a RFP retroviral vector (PT67-DsRed2), the cells were cultured in the presence of 200–1000 μg/ml G418 (Life Technologies, Inc.) for 7 days.

Production of Histone H2B-GFP Vector (26). The histone *H2B* gene has no stop codon, thereby enabling the ligation of the *H2B* gene to the 5′-coding region of the *A. victoria EGFP* gene (Clontech Laboratories, Inc.). The histone H2B-GFP fusion gene was then inserted at the *Hin*dIII/ClaI site of the pLHCX (Clontech Laboratories, Inc.) that has the hygromycin resistance gene. To establish a packaging cell clone producing high amounts of a histone H2B-GFP retroviral vector, the pLHCX histone H2B-GFP plasmid was transfected in PT67 cells using the same methods described above for PT67-DsRed2. The transfected cells were cultured in the presence of 200–400 μg/ml hygromicyn (Life Technologies, Inc.) for 15 days to establish stable PT67 H2B-GFP packaging cells.

RFP and Histone H2B-GFP Gene Transduction of Fibrosarcoma Cells. For RFP and H2B-GFP gene transduction, 70% confluent human HT-1080 fibrosarcoma cells were used. To establish dual-color cells, clones of HT-1080 expressing RFP in the cytoplasm (HT-1080-RFP) were initially established. In brief, HT-1080 cells were incubated with a 1:1 precipitated mixture of retroviral supernatants of PT67-RFP cells and RPMI 1640 (Mediatech, Inc., Herndon, VA) containing 10% FBS for 72 h. Fresh medium was replenished at this time. Cells were harvested with trypsin/EDTA 72 h post-transduction and subcultured at a ratio of 1:15 into selective medium, which contained 200 μg/ml G418. The level of G418 was increased stepwise up to 800 μg/ml. HT-1080-RFP cells were isolated with cloning cylinders (Bel-Art Products, Pequannock, NJ) using trypsin/EDTA and amplified by conventional culture methods.

For establishing dual-color cells, HT-1080-RFP cells were then incubated with a 1:1 precipitated mixture of retroviral supernatants of PT67 H2B-GFP cells and culture medium. To select the double transformants, cells were incubated with hygromycin 72 h after transfection. The level of hygromycin was increased stepwise up to 400 μg/ml. Clones HT-1080-dual-color-1 and HT-1080-dual-color-6 were isolated with cloning cylinders under fluorescence microscopy. These two clones were amplified by conventional culture methods. These sublines stably expressed GFP in the nucleus and RFP in cytoplasm.

Proliferation of Parental and Fluorescent Protein-Labeled Cells. Each fluorescent-tagged HT-1080 clone (HT-1080-RFP, HT-1080-dual-color-1, and HT-1080-dual-color-6) and parental clone (HT-1080) was seeded at a density of 1×10^3 cells/dish in 100-mm dishes with RPMI with 10% FBS medium (day 1). The dishes were kept in an incubator at 37°C and 5% CO_2. Every other day (days 2–7), three dishes for each clone were used for cell counting. In brief, resuspended cells collected after trypsinization were stained with trypan

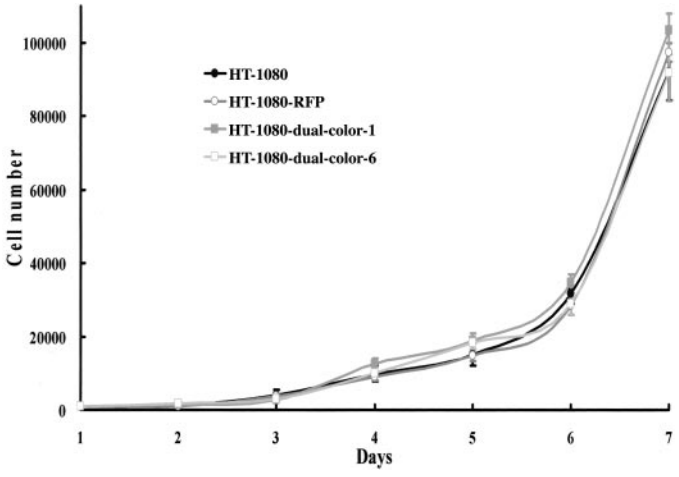

Fig. 2. Cell proliferation potential of parental and fluorescent-protein expressing clones. Three dishes for each clone (parental HT-1080, HT-1080-RFP, HT-1080-dual-color-1, and HT-1080-dual-color-6) were used at each time point for cell counts. Cells were trypsinized, stained with trypan blue, and counted in a hemocytometer. ●, the average cell number for each group.

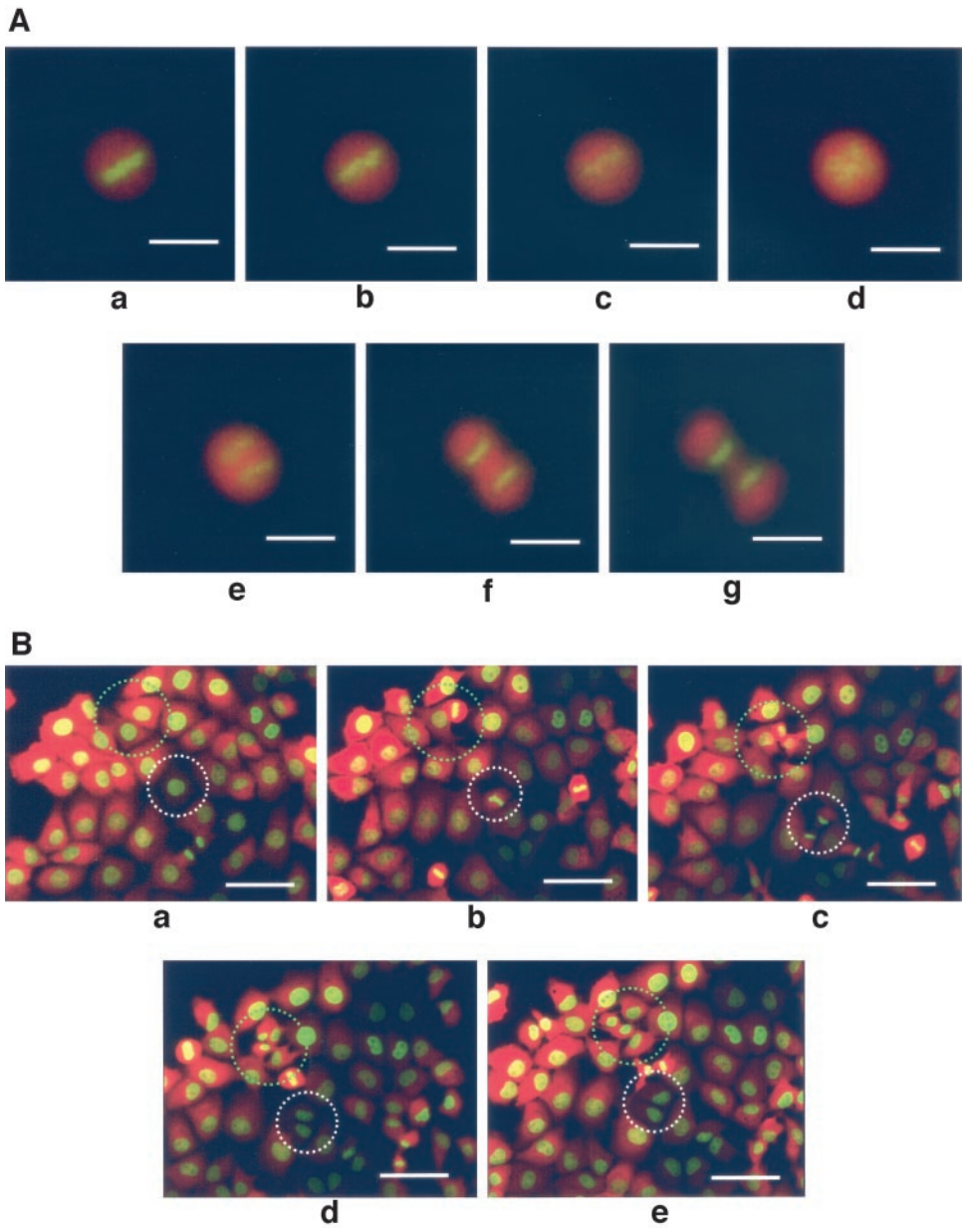

Fig. 3. Visualization of time course of mitosis *in vitro*. HT-1080-dual-color-1 cells were cultured in RPMI 1640 supplemented with 10% FBS. *A*, images were captured from the same cell under fluorescence microscopy at various time points: *a*, 0 time; *b*, 5 min; *c*, 10 min; *d*, 15 min; *e*, 20 min; *f*, 25 min; *g*, 30 min. *Bars* = 20 μm. *B*, *green* and *white circles* indicate representative areas where mitotic cells were observed. *a*, 0 time; *b*, 30 min; *c*, 60 min; *d*, 90 min; *e*, 120 min. *Bars* = 75 μm.

blue (Sigma). Only viable cells were counted with a hemocytometer (Reichert Scientific Instruments, Buffalo, NY) subsequently.

Visualization of Cell Cycle in Live HT-1080-Dual-Color Cells. HT-1080-dual-color-1 cells were cultured in 150-mm dishes with RPMI 1640 with 10% FCS. The cells were visualized under fluorescence microscopy every 5–30 min.

Visualization of Apoptotic Process in Live HT-1080 Dual-Color Cells. To visualize the apoptotic processes in real time, the HT-1080-dual-color-6 clone was used. Staurosporine (Refs. 30 and 31; Alexis, San Diego, CA), dissolved in DMSO, was used for induction of apoptosis. Cells (3×10^5) were seeded in a 25-cm^2 flask with RPMI 1640 with 10% FBS. Staurosporine was added the next day at a concentration of 2 μM. Every 2 h, the cells were visualized under fluorescence microscopy.

Real-Time Visualization of Deformability of HT-1080 Dual-Color Cells in the Brain of Live Mice. To visualize cell dynamics in the brain of living mice, cells were injected in the common carotid artery. Nude mice were anesthetized with a ketamine mixture (10 μl ketamine HCl, 7.6 μl xylazine, 2.4 μl acepromazine maleate, and 10 μl H_2O) via s.c. injection. A longitudinal skin incision was made on the neck. After exposing the submandibular gland, it was cut in the middle and retracted to each side. The right sternohyoid muscle and right sternomastoideus muscle and connective tissue were separated with a blunt instrument. After isolation of the right common carotid artery, the artery was gently released from surrounding connective tissue. Light tension was put on the proximal site of the artery with a blunt-end hook (Fine Science Tools, Inc., Foster City, CA). A total of 200 μl of medium containing 2×10^5 HT-1080-dual-color-1 cells were injected in the artery using a 33-gauge needle (Fine Science Tools). Immediately after injection, the injected site was pressed with a swab to prevent bleeding or leakage of injected tumor cells. The skin was then closed with a 6-0 suture. All procedures of the operation described above were performed with a $\times 7$ dissection microscope (MZ6; Leica, Deerfield, IL).

Scalp Flap Window. Tumor cells in the brain were visualized through the skull via a skin-flap window. The animals were anesthetized with the ketamine mixture. An arc-shaped incision was made in the scalp, and s.c. connective tissue was separated to free the skin flap. The skin flap could be opened repeatedly to image tumor cells in the brain through the nearly transparent mouse skull and simply closed with a 6-0 suture. This procedure greatly reduced the scatter of fluorescent photons.

Whole-Body Real-Time Visualization of Nuclear-Cytoplasmic Dynamics. To visualize nuclear cytoplasmic dynamics by whole-body imaging, mice were anesthetized with the ketamine mixture, and HT-1080 dual-color cells

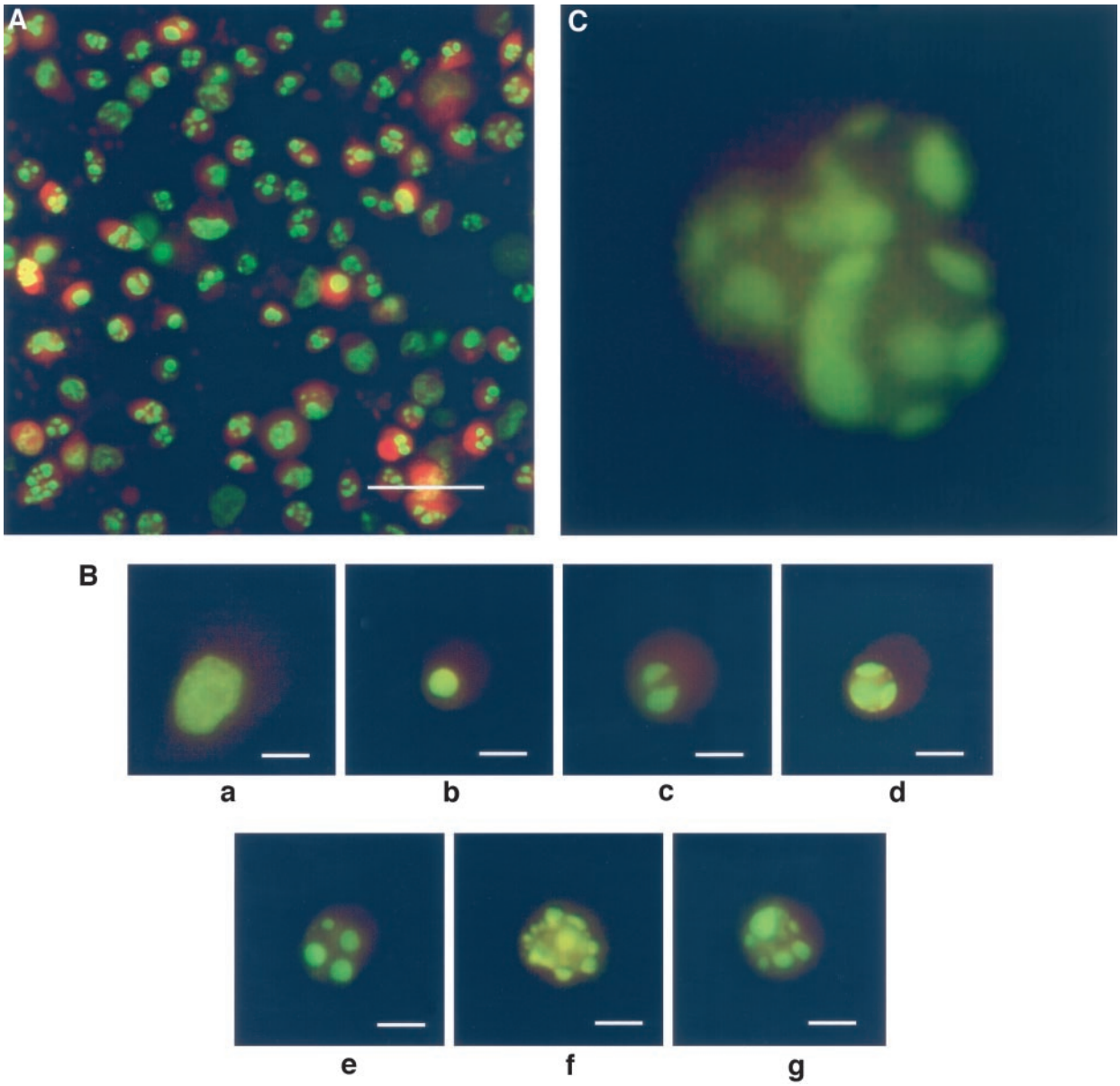

Fig. 4. Real-time visualization of apoptosis induced by staurosporine. HT-1080-dual-color-6 cells were incubated with 2 μM staurosporine. *A*, 12 h after 2 μM staurosporine treatment. Apoptosis was induced in HT-1080-dual-color cells at a high frequency. *Bar* = 50 μm. *B*, real-time high-magnification images of a single HT-1080-dual-color-6 cell in apoptosis after treatment with 2 μM staurosporine. *a*, no treatment; *b*, 2 h; *c*, 4 h; *d*, 6 h; *e*, 8 h; *f*, 10 h; *g*, 12 h. C, apoptotic HT-1080 dual-color cells with numerous nuclear fragments. *Bar* = 10 μm.

were injected in the ear of the mouse. The surface of the ear of the intact animal was directly observed under fluorescence microscopy.

Nuclear Cytoplasmic Dynamics in Lung Metastasis. Nude mice received injections of 1×10^6 HT-1080-dual-color cells in 300 μl in the tail vein. At various time points, mice were sacrificed and lungs were removed. The metastatic colonies on the lung were visualized directly under fluorescence microscopy.

Fluorescence Optical Imaging (32). Images were captured directly with a Hamamatsu C5810 3CCD camera (Hamamatsu Photonics, Bridgewater, NJ). For micro-imaging, a Leica fluorescence stereo microscope (model LZ12) was coupled with the Hamamatsu CCD camera. This microscope was equipped with a GFP filter set and a mercury lamp (Chroma Technology, Brattleboro, VT) with a 50-W power supply. Images were processed for contrast and brightness and analyzed with the use of Image ProPlus 3.1 software. High-resolution images (1024 $\times$ 724 pixel) were captured directly on an IBM PC 40.

All animal studies were conducted in accordance with the principles and procedures outlined in the NIH Guide for the Care and Use of Laboratory Animals under assurance of number A3873-1. Animals were kept in a barrier facility under HEPA filtration. Mice were fed with autoclaved laboratory rodent diet (Tecklad LM-485, Western Research Products, Orange, CA).

RESULTS AND DISCUSSION

Cell Proliferation Rates of Parental, HT-1080-RFP, and HT-1080-RFP-GFP-Dual-Color Clones. The selected HT-1080-dual-color cells have bright GFP and RFP fluorescence *in vitro* (Fig. 1). Green fluorescence is localized in the nuclei; red fluorescence is localized in the cytoplasm. All cells in the population expressed both GFP and RFP, indicating stability of both transgenes (Fig. 1). There was no difference in the proliferation rates of parental HT-1080, HT-1080-RFP, HT-1080-dual-color-1, or HT-1080-dual-color-6 clones determined in monolayer culture (Fig. 2), indicating that expression of GFP and/or RFP did not affect cell cycle progression.

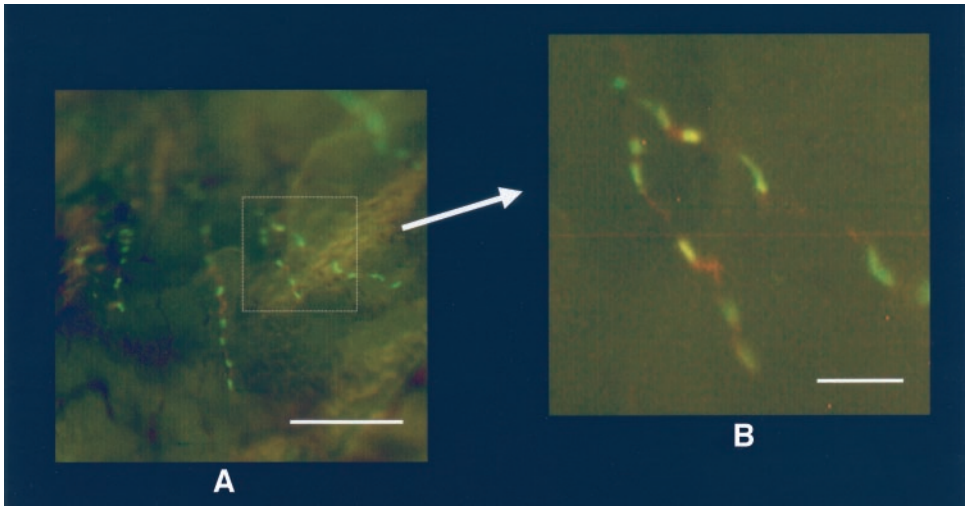

Fig. 5. Visualization of tumor cells in the brain of live mice. HT-1080-dual-color-1 cells were injected in the common carotid artery. HT-1080 dual-color cells were immediately visualized in microvessels through the skull with a skin flap window. The cell morphology and the morphology of the nuclei of each cell are visualized, and both showed extreme deformability to fit in the microvessel. *A*, low-magnification view. *Bar* = 400 μm. □, the area whose high magnification view is shown in *B*. *B*, high-magnification view. *Bar* = 100 μm.

Real-Time Visualization of Mitosis *in Vitro*. Fig. 3*A* shows a series of images of a single HT-1080 dual-color-1-cell during mitosis at 5-min intervals. A metaphase cell progressing through anaphase and cytokinesis is visualized by the green nucleus and red cytoplasm in real time. Fig. 3*B* shows cells in a dense population going through mitosis at 35-min intervals, in which they are readily followed even as they changed positions in the population.

Real-Time Observation of Apoptotic Induction *in Vitro*. Staurosporine at 2 μM induced apoptosis in HT-1080-dual-color-6 cells. (Fig. 4). In Fig. 4*A*, numerous live HT-1080-dual-color cells with fragmented nuclei are visualized. In Fig. 4*B*, progressive fragmentation of a nucleus of a single cell could be observed every 2 h in real time. The nucleus appears to first condense, then fragments in two, and then continues to form numerous additional fragments during the observation period. Fig. 4*C* visualizes a live HT1080 dual-color apoptotic cell with more than 10 nuclear fragments.

Real-Time Observation of Nuclear Cytoplasmic Deformability in the Brain. After common carotid-artery injection of HT-1080-dual-color cells, they were visualized through the skull via a scalp flap in a brain microvessel (Fig. 5, *A* and *B*). The cell body and nucleus of the dual-color tumor cells were greatly elongated to fit in small-diameter microvessels, showing the extreme deformability of both the nucleus and cytoplasm.

Whole-Body Real-Time Imaging of Mitosis. Real-time images of mitotic cells could be captured in the ear of a live mouse 12 h after the injection of HT-1080-dual-color-1 cells (Fig. 6, *A* and *B*). The cells appeared to be extravasated and were rounded, similar to dividing cells in culture. The shape of each nucleus, the high nuclear-cytoplasmic ratio, and the boundary of the cells were clearly visualized by dual-color whole-body imaging in the living animal.

Visualization of Nuclear Cytoplasmic Dynamics in Lung Metastasis. Micrometastases of HT-1080 dual-color cells on excised lungs were visualized (Fig. 7). The cells appear to be distorted to enable close contact between nuclei, suggesting intimate relationships between the cells.

This study opens up the possibility of real-time observation of tumor cell nuclear-cytoplasmic dynamics including the apoptotic process at the cellular level *in vivo* as well as *in vitro*. Mitotic cells were readily visualized after injection in the ear of live mice. After common carotid artery injection, highly elongated cells with highly elongated nuclei were observed in brain microvessels, suggesting the extreme deformability of both the cell body and nucleus. After tail-vein injection, dual-color micrometastases were visualized in excised lungs in which nuclei were juxtaposed, suggesting a novel type of cellular interaction. These observations could not have been possible without the dual-color fluorescence of the cells, which enables a novel

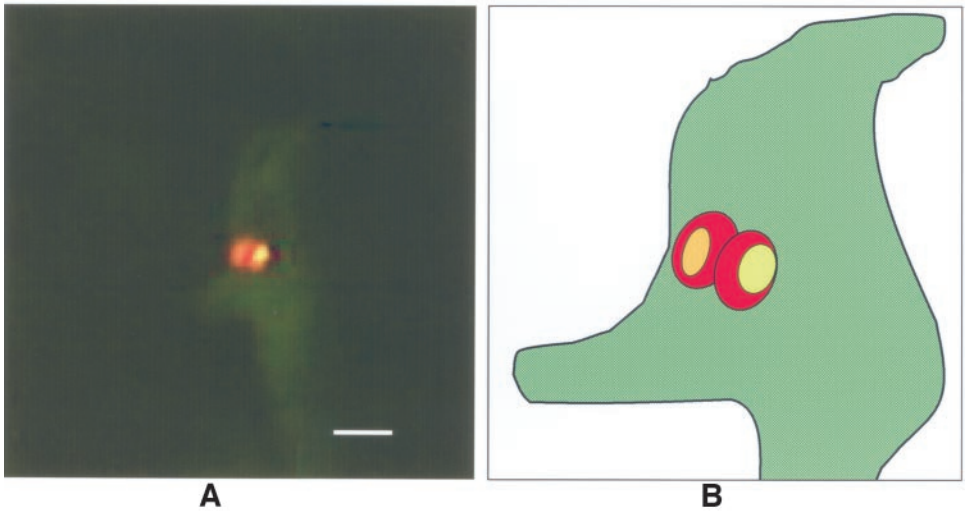

Fig. 6. Real-time whole-body image of mitotic cell in ear of a live mouse. Real-time image of mitotic tumor cells in the ear of a live mouse captured 12 h after cell injection. *A*, high-magnification image. *Bar* = 50 μm. *B*, schema of A. See "Materials and Methods" for details.

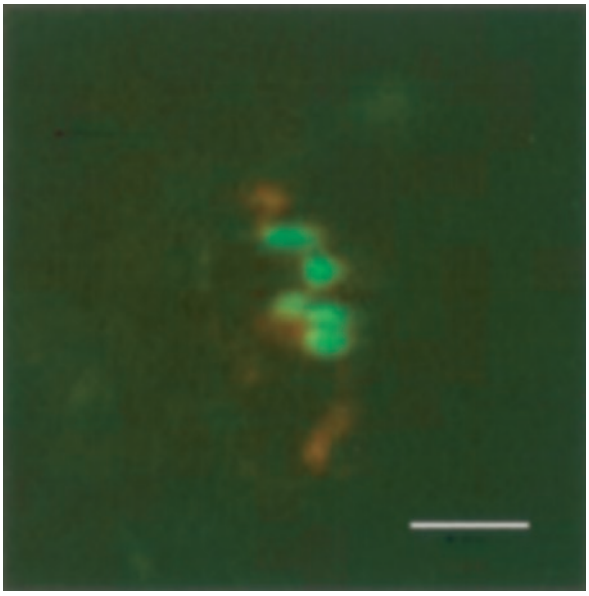

Fig. 7. Nuclear cytoplasmic dynamics in lung metastases. HT-1080-dual-color-1 cells were injected in the tail vein. Micrometastases on the lung surface are shown with nuclear-cytoplasmic morphology visualized under fluorescence microscopy. *Bar* = 30 μm.

approach to cell biology *in vivo* as well as *in vitro*. Future experiments include high-resolution observations of nuclear-cytoplasmic dynamics in dual-color cells, including visualization of chromatin dynamics in cells in the intact animal (27).

REFERENCES

1. Chambers AF, Groom AC, MacDonald IC. Dissemination and growth of cancer cells in metastatic sites. Nat Rev Cancer 2002;2:563–72.
2. Lin WC, Pretlow TP, Pretlow TG II, Culp LA. Bacterial lacZ gene as a highly sensitive marker to detect micrometastasis formation during tumor progression. Cancer Res 1990;50:2808–17.
3. Brown EB, Campbell RB, Tsuzuki Y, et al. In vivo measurement of gene expression, angiogenesis and physiological function in tumors using multiphoton laser scanning microscopy. Nat Med 2001;7:864–8.
4. Ciancio SJ, Coburn M, Hornsby PJ. Cutaneous window for in vivo observations of organs and angiogenesis. J Surg Res 2000;92:228–32.
5. Naumov GN, Wilson SM, MacDonald IC, et al. Cellular expression of green fluorescent protein, coupled with high-resolution in vivo videomicroscopy, to monitor steps in tumor metastasis. J Cell Sci 1999;112:1835–42.
6. Contag CH, Jenkins D, Contag PR, Negrin RS. Use of reporter genes for optical measurements of neoplastic disease in vivo. Neoplasia 2000;2:41–52.
7. Burgos JS, Rosol M, Moats RA, et al. Time course of bioluminescent signal in orthotopic and heterotopic brain tumors in nude mice. BioTechniques 2003;34:1184–8.
8. Prasher DC, Eckenrode VK, Ward WW, et al. Primary structure of the *Aequorea victoria* green-fluorescent protein. Gene 1992;111:229–33.
9. Chalfie M, Tu Y, Euskirchen G, et al. Green fluorescent protein as a marker for gene expression. Science 1994;263:802–5.
10. Cheng L, Fu J, Tsukamoto A, Hawley RG. Use of green fluorescent protein variants to monitor gene transfer and expression in mammalian cells. Nat Biotechnol 1996;14:606–9.
11. Cody CW, Prasher DC, Westler WM, et al. Chemical structure of the hexapeptide chromophore of the Aequorea green fluorescent protein. Biochemistry 1993;32:1212–8.
12. Yang F, Moss LG, Phillips GN Jr. The molecular structure of green fluorescent protein. Nat Biotechnol 1996;14:1246–51.
13. Morin J, Hastings J. Energy transfer in a bioluminescent system. J Cell Physiol 1971;77:313–8.
14. Cormack B, Valdivia R, Falkow S. FACS-optimized mutants of the green fluorescent protein (GFP). Gene 1996;173:33–8.
15. Crameri A, Whitehorn EA, Tate E, Stemmer WP. Improved green fluorescent protein by molecular evolution using DNA shuffling. Nat Biotechnol 1996;14:315–9.
16. Delagrave S, Hawtin RE, Silva CM, et al. Red-shifted excitation mutants of the green fluorescent protein. Biotechnology 1995;13:151–4.
17. Heim R, Cubitt AB, Tsien RY. Improved green fluorescence. Nature 1995;373:663–4.
18. Zolotukhin S, Potter M, Hauswirth WW, et al. A 'humanized' green fluorescent protein cDNA adapted for high-level expression in mammalian cells. J Virol 1996;70:4646–54.
19. Gross LA, Baird GS, Hoffman RC, et al. The structure of the chromophore within DsRed, a red fluorescent protein from coral. Proc Natl Acad Sci USA 2000;97:11990–5.
20. Fradkov AF, Chen Y, Ding L, et al. Novel fluorescent protein from Discosoma coral and its mutants possesses a unique far-red fluorescence. FEBS Lett 2000;479:127–30.
21. Hoffman RM. Green fluorescent protein imaging of tumor growth, metastasis, and angiogenesis in mouse models. Lancet Oncol 2002;3:546–56.
22. Robinett CC, Straight A, Li G, et al. In vivo localization of DNA sequences and visualization of large-scale chromatin organization using lac operator/repressor recognition. J Cell Biol 1996;135:1685–700.
23. Straight AF, Belmont AS, Robinett CC, Murray AW. GFP tagging of budding yeast chromosomes reveals that protein-protein interactions can mediate sister chromatid cohesion. Curr Biol 1996;6:1599–608.
24. Shelby RD, Hahn KM, Sullivan KF. Dynamic elastic behavior of α-satellite DNA domains visualized in situ in living human cells. J Cell Biol 1996;135:545–57.
25. Flach J, Bossie M, Bogel J, et al. A yeast RNA-binding protein shuttles between the nucleus and the cytoplasm. Mol Cell Biol 1994;14:8399–407.
26. Kanda T, Sullivan KF, Wahl GM. Histone-GFP fusion protein enables sensitive analysis of chromosome dynamics in living mammalian cells. Curr Biol 1998;8:377–85.
27. Manders EM, Visser AE, Koppen A, et al. Four-dimensional imaging of chromatin dynamics during the assembly of the interphase nucleus. Chromosome Res 2003;11:537–47.
28. Chambers AF, Schmidt EE, MacDonald IC, Morris VL, Groom AC. Early steps in hematogenous metastasis of B16F1 melanoma cells in chick embryos studied by high-resolution intravital videomicroscopy. J Natl Cancer Inst 1992;84:797–803.
29. Yamamoto N, Yang M, Jiang P, et al. Real-time imaging of individual fluorescent proteins color-coded metastatic colonies in vivo. Clin Exp Metastasis 2003;20:633–8.
30. Susin SA, Lorenzo HK, Zamzami N, et al. Mitochondrial release of caspase-2 and -9 during the apoptotic process. J Exp Med 1999;189:381–94.
31. Susin SA, Lorenzo HK, Zamzami N, et al. Molecular characterization of mitochondrial apoptosis-inducing factor. Nature 1999;397:441–6.
32. Yang M, Baranov E, Wang J-W, et al. Direct external imaging of nascent cancer, tumor progression, angiogenesis, and metastasis on internal organs in the fluorescent orthotopic model. Proc Natl Acad Sci USA 2002;99:3824–9.